https://doi.org/10.5194/acp-2021-389
Preprint. Discussion started: 31 May 2021

Atmospheric Chemistry and Physics Discussions

Formaldehyde evolution in U.S. wildfire plumes during FIREX-AQ

Jin Liao[1,2], Glenn M. Wolfe[1], Reem A. Hannun[1,3], Jason M. St. Clair[1,3], Thomas F. Hanisco[1], Jessica B. Gilman[4], Aaron Lamplugh[4,5], Vanessa Selimovic[6], Glenn S. Diskin[7], John B. Nowak[7], Hannah S. Halliday[8], Joshua P. DiGangi[7], Samuel R. Hall[9], Kirk Ullmann[9], Christopher D. Holmes[10], Charles H. Fite[10], Anxhelo Agastra[10], Thomas B. Ryerson[4,*], Jeff Peischl[4,5], Ilann Bourgeois[4,5], Carsten Warneke[4], Matthew M. Coggon[4,5], Georgios I. Gkatzelis[4,5,**], Kanako Sekimoto[11], Alan Fried[12], Dirk Richter[12], Petter Weibring[12], Eric C. Apel[9], Rebecca S. Hornbrook[9], Steven S. Brown[4], Caroline C. Womack[4,5], Michael A. Robinson[4,5], Rebecca A. Washenfelder[4], Patrick R. Veres[4], J. Andrew Neuman[4,5]

[1]Atmospheric Chemistry and Dynamics Laboratory, NASA Goddard Space Flight Center, Greenbelt, MD, USA

[2]Universities Space Research Association, Columbia, MD, USA

[3]Joint Center for Earth Systems Technology, University of Maryland Baltimore County, Baltimore, MD, USA

[4]NOAA Chemical Science Laboratory (CSL), Boulder, CO, USA

[5]Cooperative Institute for Research in Environmental Science (CIRES), University of Colorado, Boulder, CO, USA

[6]Department of Chemistry, University of Montana, Missoula, MT, USA

[7]NASA Langley Research Center, Hampton, VA, USA

[8]Environmental Protection Agency, Durham, NC, USA

https://doi.org/10.5194/acp-2021-389
Preprint. Discussion started: 31 May 2021

Atmospheric Chemistry and Physics Discussions

[9]Atmospheric Chemistry Observations & Modeling Laboratory, National Center for Atmospheric Research, Boulder, CO, USA

[10]Earth, Ocean and Atmospheric Science, Florida State University, FL, USA

[11]Yokohama City University, Japan

[12]Institute of Arctic and Alpine Research (INSTAAR), University of Colorado, Colorado, USA.

[*]now at Scientific Aviation, Boulder, Colorado, USA.

[**]now at Forschungszentrum Jülich GmbH, Julich, Nordrhein-Westfalen, DE, Germany.

Correspondence email: jin.liao@nasa.gov

https://doi.org/10.5194/acp-2021-389
Preprint. Discussion started: 31 May 2021

Atmospheric Chemistry and Physics Discussions

Abstract

Formaldehyde (HCHO) is one of the most abundant non-methane volatile organic compounds (VOCs) emitted by fires. HCHO also undergoes chemical production and loss as a fire plume ages, and it can be an important oxidant precursor. In this study, we disentangle the processes controlling HCHO by examining its evolution in wildfire plumes sampled by the NASA DC-8 during the FIREX-AQ field campaign. In nine of the twelve analyzed plumes, dilution-normalized HCHO increases with physical age (range 1 – 6 h). The balance of HCHO loss (mainly via photolysis) and production (via OH-initiated VOC oxidation) controls the sign and magnitude of this trend. Plume-average OH concentrations, calculated from VOC decays, range from –0.5 ($\pm$ 0.5) × 10^6 to 5.3 ($\pm$0.7) × 10^6 cm^{-3}. Plume-to-plume variability in dilution-normalized secondary HCHO production correlates with OH abundance rather than normalized OH reactivity, suggesting that OH is the main driver of fire-to-fire variability in HCHO secondary production. Analysis suggests an effective HCHO yield of 0.33 ($\pm$ 0.05) per VOC molecule oxidized for the 12 wildfire plumes. This finding can help connect space-based HCHO observations to the oxidizing capacity of the atmosphere.

https://doi.org/10.5194/acp-2021-389
Preprint. Discussion started: 31 May 2021

Atmospheric Chemistry and Physics Discussions

1. Introduction

Wildfire biomass burning is a large source of trace gases and aerosols that affect regional atmospheric chemistry, human health, air quality, radiative balance and climate. Wildfire frequency and intensity are expected to increase with global warming under higher temperatures and drier conditions in the future (Westerling et al., 2006). Wildfire emissions of volatile organic compounds (VOCs) are a complex mixture spanning orders of magnitude in concentration, reactivity, and volatility (Gilman et al., 2015; Koss et al., 2018). These VOCs contribute to increased regional tropospheric ozone (Alvarado et al., 2010; Jaffe and Wigder, 2012; Mauzerall et al., 1998; Wotawa and Trainer, 2000) and can deposit onto or evaporate from organic aerosols in biomass burning air masses (Garofalo et al., 2019; Majdi et al., 2019; Palm et al., 2020).

Formaldehyde (HCHO) is one of the most abundant non-methane VOCs emitted by wildfires (Akagi et al., 2011; Gilman et al., 2015; Simpson et al., 2011). HCHO emissions vary with total carbon emissions, modified combustion efficiency (MCE) and fuel type. Emission factors of HCHO decrease as MCE increases (e.g., Liu et al., 2017; Yokelson et al., 1999), indicating that more HCHO is produced from smoldering fires than from flaming fires. HCHO emissions can vary by more than a factor of 2 among tropical forest, savanna, boreal forest and temperate forest biomes (Akagi et al., 2011). In addition to direct emissions, HCHO is formed in fire plumes via VOC oxidation. Alvarado et al. (2020) used TROPOMI data to show that HCHO enhancements in wildfire plumes persist for days downwind. HCHO also serves as an important source of peroxy radicals (HO_2), thereby influencing the formation of ozone and other secondary pollutants (Yokelson et al., 1999).

https://doi.org/10.5194/acp-2021-389
Preprint. Discussion started: 31 May 2021


Atmospheric Chemistry and Physics Discussions

70

71 Few studies have investigated the photochemical evolution of HCHO in biomass burning plumes,
72 and these studies have reported both net HCHO production and loss. Mauzerall et al. (1998)
73 reported average HCHO enhancement (ΔHCHO/ΔCO) of 9.5 ppt/ppb for fresh plumes (less than
74 0.5 day), 1.8 ppt/ppb for recent plumes (less than 1 day), 2.3 ppt/ppb for aged plumes (< 5 days
75 old), and 0.9 ppt/ppb for old plumes (>5 days old). Trentmann et al. (2005) observed a potential
76 increasing trend of ΔHCHO/ΔCO from 20 ppt/ppb to over 30 ppt/ppb with limited data and
77 simulated a flat trend of ΔHCHO/ΔCO within 1 h age since emission from a Savanna fire plume
78 in Africa. Müller et al. (2016) also observed an increasing trend of ΔHCHO/ΔCO with an average
79 of 22.7 ppt/ppb and simulated a flat or slightly decreasing trend of ΔHCHO/ΔCO in a small fresh
80 agricultural biomass burning plume in Georgia, US. While such case studies are valuable, we lack
81 a general understanding of the drivers of plume trends and plume-to-plume variability in HCHO
82 evolution.

83

84 HCHO is also one of the few VOCs that can be observed from space, and the global coverage of
85 satellite observations has been leveraged to provide insights into a variety of atmospheric
86 chemistry questions. HCHO is correlated with organic aerosols in biomass burning air masses, and
87 this correlation might be exploited to estimate organic aerosol abundance from satellite HCHO
88 measurements (Liao et al., 2019). In regions with constant or very high OH reactivity, HCHO
89 variability is closely linked to OH variability (Valin et al., 2016; Wolfe et al., 2019) and may be
90 used to infer OH. Satellite HCHO columns have also been widely used to constrain emissions of
91 isoprene and other VOCs (Fu et al., 2007; Kaiser et al., 2018; Marais et al., 2014; Millet et al.,
92 2008; Stavrakou et al., 2009). Understanding the emissions, chemistry and trends of HCHO in

https://doi.org/10.5194/acp-2021-389
Preprint. Discussion started: 31 May 2021


Atmospheric Chemistry and Physics Discussions

93 wildfires will facilitate the application of satellite HCHO towards broad-scale wildfire smoke
94 processes and impacts.
95
96 The Fire Influence on Regional to Global Environments and Air Quality experiment (FIREX-AQ)
97 deployed a comprehensive suite of instruments aboard the NASA DC-8 aircraft to study wildfires
98 and agricultural fires in the US. It provided a great opportunity to systematically study the
99 emissions and chemistry of HCHO in wildfire plumes. In the following, we describe the HCHO
100 dependence on plume age in wildfire plumes from FIREX-AQ, assess the drivers of HCHO trends,
101 and examine the factors controlling variability in secondary HCHO production.
102
103 2. Methods
104 2.1 FIREX-AQ field campaign and measurements description
105 During FIREX-AQ, a combination of four aircraft (the NASA DC-8, NASA ER-2, and two
106 NOAA Twin Otters) with a comprehensive suite of in situ and remote sensing instruments were
107 deployed to characterize fire emissions and chemistry with operational bases in Boise, ID and
108 Salina, KS from July to September 2019. This study focuses on wildfire plumes sampled by the
109 NASA DC-8 aircraft during FIREX-AQ.
110
111 In situ HCHO observations were acquired by several instruments onboard the DC-8; here we
112 primarily use measurements from the In Situ Airborne Formaldehyde (ISAF) instrument (Cazorla
113 et al., 2015). ISAF uses laser-induced fluorescence to detect HCHO. A tunable UV laser excites
114 HCHO molecules to an excited electronic state and the resulting fluorescence is detected with a
115 photon-counting photomultiplier tube. The laser wavelength is modulated on and off a rotational

https://doi.org/10.5194/acp-2021-389
Preprint. Discussion started: 31 May 2021


Atmospheric Chemistry and Physics Discussions

116 absorption feature (353.163 nm), and the difference between the "online" and "offline" signals is
117 proportional to the HCHO concentration.
118
119 ISAF was calibrated pre- and post-mission with a compressed-gas HCHO cylinder (584 ± 15 ppbv
120 in nitrogen, Air Liquide). Sensitivity typically varies by less than 5% between calibrations. Flow
121 meters for the standard dilution system were calibrated against a DryCal calibrator (Mesa Labs)
122 with an accuracy of < 1%. The HCHO standard concentration was calibrated before and after the
123 field deployment with an MKS Multigas 2031 Fourier transform infrared spectrometer. Gas
124 standard mixing ratios are typically reproducible to within 2% of the mean value measured over
125 multiple years. IR-determined mixing ratios are adjusted by a factor of 0.96 based on a separate
126 long-path UV absorption experiment (Cazorla et al., 2015). Thus, ISAF HCHO mixing ratios are
127 ultimately tied to the UV cross sections of Meller and Moortgat (2000) as recommended by the
128 JPL 2011 evaluation (Sander et al., 2011). The detection limit of ISAF was 30 pptv for 1-Hz data
129 at signal/noise = 1 and the accuracy of ISAF HCHO measurements was estimated as 10% + 10
130 pptv. The 1/*e* response time of ISAF during FIREX-AQ was about 300 ms, limited mainly by
131 flow through the sample cell.
132
133 During FIREX-AQ, ISAF HCHO measurements correlated with those from the Compact
134 Atmospheric Multispecies Spectrometer (CAMS) (Richter et al., 2015), with a correlation
135 coefficient r^2 of 0.99, a slope of 1.27 (CAMS vs. ISAF), and a near-zero intercept for 1-Hz average
136 wildfire data from equally weighted orthogonal distance regression (Fig. S1). The systematic bias
137 between the CAMS and ISAF measurements exceeds the combined stated uncertainty (10% for
138 ISAF, 6% for CAMS). Post-mission comparisons suggest this discrepancy is due to the absolute

https://doi.org/10.5194/acp-2021-389
Preprint. Discussion started: 31 May 2021


Atmospheric Chemistry and Physics Discussions

calibration of compressed-gas HCHO standards, which are tied to literature-recommended UV (ISAF) or IR (CAMS) cross sections; the source of this discrepancy is still under investigation. Remotely-sensed HCHO column retrievals rely on the same UV cross sections (De Smedt et al., 2018) that are used to calibrate the ISAF instrument. The HCHO enhancements in the plumes (Sect 3.1) and the estimated effective yield of HCHO from VOC oxidation by OH (Sect. 3.3) can have a potential low bias of 27% due to the ISAF and CAMS HCHO measurement difference. This uncertainty proportionally affects quantitative analysis results but does not alter qualitative conclusions.

We also use several supporting measurements in our analysis. CO was measured via mid-IR wavelength modulation spectroscopy by the Differential Absorption Carbon Monoxide Measurement (DACOM) instrument (Sachse et al., 1991). Photolysis rates were derived from the Actinic flux measurements by the Charged-coupled device Actinic Flux Spectroradiometer (CAFS) (Hall et al., 2018). Alkenes were measured by the NOAA Whole Air Sampler (iWAS) (Lerner et al., 2017). Ozone (O_3) measurements were from the NOAA Chemiluminescence instrument (Bourgeois et al., 2020). OH reactivity calculations used VOCs measurements from the NOAA Proton-Transfer Reaction Time-of-Flight Mass Spectrometry (PTR-ToF-MS) (Yuan et al., 2016), NCAR Trace Organic Gas Analyzer (TOGA) (Apel et al., 2015) outfitted with a Time-of-Flight Mass Spectrometer, NOAA Airborne Cavity Enhanced Spectrometer (ACES) (Min et al., 2016), and NOAA Iodide Ion Time-of-Flight (ToF) Chemical Ionization Mass Spectrometer (CIMS) (Veres et al., 2020), listed in Table S1. Our analysis uses in situ measurements that are merged to the iWAS sampling period, which ranged from 1-9 seconds per canister, such that multiple samples were often acquired within a single plume crossing.

https://doi.org/10.5194/acp-2021-389
Preprint. Discussion started: 31 May 2021


Atmospheric Chemistry and Physics Discussions

162

163 2.2 Normalized excess mixing ratio (NEMR) and physical age definitions

164 NEMR is defined as the difference between the concentration of species X in the plume and in the
165 background air outside of the plume, normalized by the difference between CO concentrations in
166 the plume and the background outside of the plume.

167 $$\text{NEMR}=\frac{\Delta X}{\Delta CO} \quad (1)$$

168 The background air outside of the plumes was manually selected and could be different or the
169 same for different transects of the same plume, depending on the availability of the iWAS data.
170 The HCHO NEMR is denoted by nHCHO below.

171

172 Physical age was estimated using a Lagrangian trajectory analysis (Holmes et al., in preparation)
173 and described briefly here. Fire source locations were pinpointed using the MODIS/ASTER
174 Airborne Simulator (MASTER) instrument data onboard the DC-8. Upwind trajectories from
175 aircraft locations were computed and the advection age was calculated from the time when a
176 trajectory was closest to the fire. Plume rise time from the surface to the trajectory initialization
177 altitude assumed a vertical wind speed of 7 m/s. The smoke age is the sum of advection age plus
178 rise age averaged over several meteorological models. The average uncertainty of the estimated
179 physical age for the analyzed wildfire plumes was 37% with an interquartile range of 20% based
180 on the range of ages derived from the High-Resolution Rapid Refresh (HRRR), North American
181 Mesoscale Forecast System (NAM) CONUS Nest, and Global Forecast System (GFS 0.25°)
182 meteorological datasets.

183

184 2.3 Plume selection

https://doi.org/10.5194/acp-2021-389
Preprint. Discussion started: 31 May 2021


Atmospheric Chemistry and Physics Discussions

185 Details about the specific selected wildfire plumes among all sampled wildfire plumes during
186 FIREX-AQ are provided in Table S2. Wildfire plumes that meet the conditions listed below are
187 selected to study the evolution of HCHO in wildfires.
188 a) Lagrangian sampling patterns
189 Lagrangian sampling patterns are defined as flight tracks intercepted the plumes with flight leg
190 directions approximately perpendicular to the horizontal wind directions and more than three
191 transects downwind with different distances from the fire.
192 b) Enhanced HCHO mixing ratios above background
193 We selected the plumes with maximum 1-Hz HCHO mixing ratios > 600 ppt, which was close to
194 the ambient background HCHO mixing ratios. The North Hill plume on 29 July 2019 is the plume
195 with the lowest HCHO concentrations among the selected plumes.
196 c) Appropriate VOC decay for the period analyzed with sufficient data samples
197 We selected the plume samples where chemical age correlated with physical age. This was defined
198 by a correlation coefficient $r^2 \geq 0.57$ for a plot of ln(trans-2-butene/propene) or ln(cis-2-
199 butene/propene) vs physical age. We used 2-butenes/propene as chemical age tracers in this
200 analysis because these gases have comparable lifetimes to physical age for most of the analyzed
201 plumes. We filtered out plume data if the correlation coefficient of ln(trans-2-butene/propene) or
202 ln(cis-2-butene/propene) vs. physical age degraded at older physical ages. Figure S2 shows
203 ln(trans-2-butene/propene) and ln(cis-2-butene/propene) vs. physical age for the plumes that
204 satisfied conditions a) and b) and had iWAS data available. The threshold of $r^2 = 0.57$ is chosen
205 by visual inspection of all VOC decay in Fig. S2. We also filtered out plumes with total number
206 of data points < 8 in the iWAS sample periods for an entire selected circuit of multiple plume
207 transects with good VOC decay. Due to the inhomogeneity of the plumes, too few data points can

https://doi.org/10.5194/acp-2021-389
Preprint. Discussion started: 31 May 2021


Atmospheric Chemistry and Physics Discussions

208 introduce large bias. In the analyzed plume periods, ln(trans-2-butene/propene) or ln(cis-2-
209 butene/propene) also has good correlations with the maleic anhydride/furan ratio (Fig. S3), another
210 tracer of chemical age in biomass burning plumes (personal communication with Carsten Warneke
211 and Matthew M. Coggon, 2021). The Mica and Lick Creek plume on 02 August 2019 is the plume
212 with the least number of data points among the selected plumes (N = 8).
213
214 The above filters, applied to a total of 26 fire plumes, yield 11 daytime plumes and 1 nighttime
215 plume that are suitable for our analysis (Table S2). One of the twelve plumes (Blackwater)
216 occurred in the southeast US and the rest eleven plumes were in the western US.
217
218 2.4 Estimating average OH concentrations in the plumes
219 Plume photochemical age is estimated based on the relative decay of primary emitted VOCs that
220 have different reaction rate coefficients with OH (e.g., Warneke et al., 2007). We can estimate the
221 average concentration of OH by combining the photochemical age with the trajectory-based air
222 mass age. Cis-2-butene/propene ratios and trans-2-butene/propene ratios are used to estimate OH
223 in this analysis because these gases have comparable lifetimes to physical age (2–6 h) for most of
224 the analyzed plumes. The lifetimes of propene, cis-2-butene, and trans-2-butene are approximately
225 4.5 h, 2.3 h, and 1.8 h, respectively, at OH concentrations of 2×10^6 molecules cm^{-3} (Atkinson et
226 al., 2006). Because both 2-butenes also differ from propene in O_3 reaction rate coefficients, the
227 reactions of these alkenes with O_3 are also considered when we estimate the OH concentrations.
228 We assume that the variability in the butenes–propene relationship is driven by OH and O_3 and
229 that there is negligible change in the relative emission ratios over the sampled plumes. These
230 reaction rate coefficients are those reported by Atkinson et al. (2006).

https://doi.org/10.5194/acp-2021-389
Preprint. Discussion started: 31 May 2021


Atmospheric Chemistry and Physics Discussions

$$\ln\frac{\text{butene}}{\text{propene}} = \ln\frac{\text{butene}_0}{\text{propene}_0} - \{(k_{\text{butene+OH}} - k_{\text{propene+OH}})[\text{OH}] + (k_{\text{butene+O}_3} - k_{\text{propene+O}_3})[\text{O}_3]\}t \quad (2)$$

OH concentrations are derived from the slope of $\ln\frac{\text{butene}}{\text{propene}}$ vs. t (physical age), the measured ozone concentrations and the reaction rate coefficients.

$$[\text{OH}] = \frac{slope_{butene} + (k_{\text{butene+O}_3} - k_{\text{propene+O}_3})[O_3]}{k_{propene+OH} - k_{butene+OH}} \quad (3)$$

The average ozone concentration of the entire circuit with multiple transects is used to represent the integrated O_3 effect on alkene oxidation. The uncertainty due to O_3 variation and the uncertainty in the slope of $\ln\frac{\text{butene}}{\text{propene}}$ vs. t are propagated to estimate the total uncertainty in plume-average OH.

2.5 Calculating primary HCHO normalized mixing ratios and secondary HCHO production rates

To understand the relative importance of primary emission vs. secondary production of HCHO in fire plumes downwind, we calculate primary and secondary HCHO as the plume ages. The primary HCHO time profile is calculated by the following equation:

$$\text{nHCHO}_{\text{primary}} = \text{nHCHO}_0 \exp(-(J_{HCHO} + k_{HCHO}[\text{OH}])t) \quad (4)$$

where nHCHO_0 is equal to the fitted observed nHCHO (HCHO NEMR) closest to the fire source, J_{HCHO} is the measured HCHO photolysis frequency in iWAS sample periods averaged and interpreted in physical age space, k_{HCHO} is the reaction rate coefficient between HCHO and OH, and t is the physical age. $\text{nHCHO}_{\text{secondary}}$ is calculated by subtracting $\text{nHCHO}_{\text{primary}}$ from the measured nHCHO. Here we assumed the fitted observed nHCHO closest to the fire source is equal to nHCHO at the emission source. This assumption will not impact the secondary nHCHO production rate calculated below.

https://doi.org/10.5194/acp-2021-389
Preprint. Discussion started: 31 May 2021


Atmospheric Chemistry and Physics Discussions

253

254 To characterize secondary HCHO production in wildfire plumes, we calculate the secondary
255 nHCHO production rate. The secondary nHCHO production rate is derived from the HCHO mass
256 balance equation.

257 $$\frac{\mathrm{d\,HCHO}}{\mathrm{dt}} = \mathrm{P} - \mathrm{L} - \mathrm{D} \quad (5)$$

258 where P is chemical production, L is chemical loss, and D is dilution. The calculation of the
259 secondary nHCHO production rate is shown in eqn. 6. The derivation of eqn. 6 from eqn. 5 can be
260 found in the Appendix A.

261 $$\frac{P}{\Delta CO}\ (\text{or } \mathrm{P_{nHCHO}}) = \frac{dnHCHO}{dt} + (\mathrm{J_{HCHO}} + \mathrm{k_{HCHO}}[OH])nHCHO. \quad (6)$$

262 Here, $\frac{d\ \mathrm{nHCHO}}{dt}$ is taken as the slope of measured nHCHO vs physical age and other parameters are
263 as defined above.

264

265 2.6 Impact of potential variation in HCHO emission ratios on nHCHO trend

266 In this analysis, we assume the variability in the HCHO/CO emission ratio (that is, nHCHO at the
267 source) is much smaller than the variability in nHCHO induced by chemistry for any single fire
268 plume. Emission factors of both HCHO and CO (that is, g of gas per kg of fuel burned) depend on
269 MCE, fuel type, and other factors (e.g., Liu et al., 2017; Yokelson et al., 1999). Normalizing
270 HCHO by CO removes the strong negative dependence of HCHO emission factors on MCE. A
271 small positive trend of nHCHO vs. MCE is due to higher nHCHO and MCE for the eastern US
272 wildfire plume than the western US wildfire plumes (Fig. S4). No clear trend of MCE in nHCHO
273 plume evolution was observed in FIREX-AQ data (Fig. S5). Emissions of CO_2 correlate with fire
274 radiative power (FRP) detected by satellite during FIREX-AQ, and the variability of FRP could
275 affect the variability of downwind concentrations (Wiggins et al., 2020). We found that HCHO

https://doi.org/10.5194/acp-2021-389
Preprint. Discussion started: 31 May 2021


Atmospheric Chemistry and Physics Discussions

276 correlates with CO_2 (Fig. S6a) and thus likely also with FRP because the change of measured CO_2
277 correlates with the change of FRP (Wiggins et al., 2020). To account for emission variation and
278 dilution, which are main factors affecting the absolution concentrations of trace gases and aerosols
279 in the plumes, HCHO is normalized to CO to investigate the impact of photochemistry on HCHO
280 evolution in the plumes. Photochemistry takes place while emission varies. When normalized to
281 CO, nHCHO does not strongly depend on CO_2 (Fig. S6b and Fig. S7) or FRP. FRP and MCE do
282 not control the trends of nHCHO.
283
284 2.7 OH reactivity calculation
285 We calculate the observed OH reactivity using the Framework for 0-D Atmospheric Modeling
286 (F0AM v4) (Wolfe et al., 2016) with the Master Chemical Mechanism v3.3.1 (MCM; Jenkin et al.,
287 2015) and additional chemical reactions from recent publications of newly-observed biomass
288 burning species and reactions (Coggon et al., 2019; Decker et al., 2019). The VOC chemical
289 species included in the F0AM model are listed in Table S1. We calculate the OH-VOC reactivity
290 ($\sum k_i VOC_i$) by excluding OH reactions with NO_2 and CO.
291
292 3. Results and discussion
293 3.1 Trends of HCHO in wildfire plumes
294 nHCHO in wildfire plumes can increase or decrease as plumes age. The trends of measured
295 nHCHO vs. physical age and the corresponding quadratic polynomial regression for 12 selected
296 plumes are plotted in Fig. 1. Quadratic polynomial regression is used because it has suitable
297 degrees of freedom to capture the trends. Considering the CO measurement uncertainty of ≤ 7%
298 and HCHO measurement uncertainty of 10%, the uncertainty of nHCHO is estimated to be ± 12%

https://doi.org/10.5194/acp-2021-389
Preprint. Discussion started: 31 May 2021


Atmospheric Chemistry and Physics Discussions

299 with a potential systematic low bias of as much as 27% (based on the difference between ISAF
300 and CAMS). Random error due to HCHO and CO measurement precision is negligible when
301 averaging over the iWAS integration time in high-concentration biomass burning plumes.
302
303 In the absence of secondary production, we expect nHCHO to decay with a time constant of a few
304 hours in the daytime. The blue curves in Fig. 1 show the predicted decay of initial nHCHO using
305 observed HCHO photolysis rates and measurement-derived OH concentrations. Because the
306 variability in nHCHO in one transect is significant, we use the start point of the observed nHCHO
307 fitted curve to represent the observed nHCHO closest to fire. HCHO photolysis frequencies are
308 averaged over each transect and linearly interpolated to determine continuous age-dependent
309 photolysis frequencies. The calculated nHCHO without production represents an upper limit of
310 primary (emitted) nHCHO because some HCHO production and loss had already occurred before
311 the closest transect.
312
313 We can also estimate the primary nHCHO (black dashed curves) and the fraction of primary
314 HCHO by assuming nHCHO and the loss rate of nHCHO were constant between emission and the
315 closest observation. The fraction of primary nHCHO to total nHCHO varies from plume to plume
316 and depends on secondary HCHO production rates and total HCHO loss rates. The primary HCHO
317 fraction could decay rapidly to be 60% in about 1 h of aging or it could decay slowly to still account
318 for 60% in about 5h of aging. The primary and secondary fractions of HCHO indicate the impact
319 of direct emission and photochemistry on the fire plume composition downwind. The average and
320 standard deviation of nHCHO production and loss rates for each plume are provided in Table S3.
321

https://doi.org/10.5194/acp-2021-389
Preprint. Discussion started: 31 May 2021


Atmospheric Chemistry and Physics Discussions

322 HCHO production exceeds loss in 9 of the 12 selected plumes, indicated by positive trends of
323 nHCHO vs. physical age in Fig. 1. Plumes exhibiting negative nHCHO trends have higher nHCHO
324 loss rates than production rates (Table S3). This shows that fire-to-fire variability in the overall
325 nHCHO trend relates to the balance between loss (via photolysis) and production (via VOC
326 oxidation). HCHO loss by photolysis can be either higher or lower than the loss by reaction with
327 OH, but on average photolysis is faster. HCHO loss via photolysis accounts for 63 ± 27% of the
328 total HCHO loss in daytime plumes. The average HCHO lifetime by photolysis was 8.2 (± 8.8) h
329 for the 11 daytime plumes, shorter than the average HCHO lifetime by OH oxidation of 23.5 (±
330 31.3) h. For some plume transects, there was significant variability in HCHO photolysis
331 frequencies over iWAS averaging intervals due to the aerosol radiative effects. Applying filters to
332 only analyze the data with relatively homogeneous in-plume HCHO photolysis rates does not alter
333 our conclusions. Plume-average OH is not well correlated with the HCHO photolysis frequency
334 (Fig. S8), likely due to inter-fire variability of OH sources and sinks.
335
336 3.2 OH concentration estimation
337 OH is the main oxidant that reacts with VOCs to produce HCHO in the daytime. As described in
338 Sect. 2.4, we estimate plume-average OH concentrations using the relative decays of 2-butenes to
339 propene via eqn. 3. The decay of the natural logarithm of the trans-2-butene to propene ratio and
340 the cis-2-butene to propene ratio with physical age are plotted in Fig. 2 with significant correlation
341 (r^2 = 0.57–0.99) for the 12 plumes. The lowest correlation coefficient occurs for the nighttime
342 plume on 12 August 2019 and the daytime plume on 29 July 2019. This indicates that the
343 photochemical age of the plumes is consistent with their physical age, and the oxidation chemistry
344 can be reasonably represented by average OH and O_3.

https://doi.org/10.5194/acp-2021-389
Preprint. Discussion started: 31 May 2021


Atmospheric Chemistry and Physics Discussions

345

346 The estimated average OH concentrations for the 12 plumes are shown in Fig. 3. The uncertainties
347 in OH concentrations are based on the standard error in the slope of ln(butenes/propene) vs
348 physical age and the standard deviation of O_3 concentrations. The average and standard deviation
349 of O_3 concentrations and the uncertainty in OH estimation due to the impact of O_3 standard
350 deviation are listed in Table S4. The variation of OH concentrations derived from trans-2-butene
351 to propene ratios is generally consistent with that derived from cis-2-butene to propene ratios,
352 though OH concentrations from trans-2-butene have slightly higher (27% on average) values than
353 that from cis-2-butene to propene, which may be due to systematic bias in the reaction rate
354 coefficients at low temperature (276.9±3.9 K). The average OH concentrations from trans-2-
355 butene to propene and cis-2-butene to propene were used to represent the average OH
356 concentrations of the plumes. OH concentrations covered a large range, varying from −0.5(±
357 0.5)× 10^6 (for a nighttime plume) to 5.3(±0.7) ×10^6 molecules cm^{-3}.

358

359 3.3 Controls on secondary HCHO formation

360 The average secondary nHCHO production rate correlates with the average OH concentration (r^2
361 = 0.69, Fig. 4a). The secondary production rates of nHCHO were calculated from the trends of
362 observed nHCHO ($\frac{dnHCHO}{dt}$), photolysis loss rate and OH (eqn. 6). The uncertainty in nHCHO
363 secondary production rates for each plume is estimated from the standard deviation of the
364 calculated nHCHO secondary production rates along the physical age of the plume. The
365 uncertainty in estimated OH is determined by the propagated uncertainties of OH from trans-2-
366 butene to propene ratios and cis-2-butene to propene ratios. The good correlations (r^2= 0.69)
367 between the secondary production rate of nHCHO and average OH indicate that the variability in

https://doi.org/10.5194/acp-2021-389
Preprint. Discussion started: 31 May 2021


Atmospheric Chemistry and Physics Discussions

368 OH is a key driver of the secondary production rate of nHCHO. Figure 4a is color-coded with
369 normalized OH-VOC reactivity calculated from measured VOCs (Sect. 2.7). Plume-average
370 normalized OH-VOC reactivity ranges from 11 to 31 s^{-1} (ppm CO)$^{-1}$, is about 20% lower than total
371 OH reactivity across the analyzed plumes, and does not exhibit a clear relationship with OH. This
372 demonstrates that variability in OH, as well as secondary nHCHO production, likely depends
373 principally on variability in OH sources (e.g., photolysis of HONO and conversion of HO_2 by NO)
374 (Peng et al., 2020) rather than sinks. Because nHCHO trend, OH concentration, and normalized
375 OH-VOC reactivity all depend on physical age, in addition to the different properties of the plumes,
376 the difference in physical age among these plumes also has an impact on the average values.
377
378 Figure 4b shows nHCHO production vs. the product of OH and dilution-normalized observed OH-
379 VOC reactivity (averaged for each plume). The latter is a lower limit for the total average OH
380 loss/production rate as observations do not include all OH sinks. The correlation is slightly higher
381 than that in Fig. 4a because variability in normalized OH-VOC reactivity plays a smaller role than
382 OH in affecting P_{nHCHO}. The slope of this relationship, 0.33 ± 0.05, is a metric for the effective
383 yield of HCHO from OH-initiated VOC oxidation. Assuming that reaction of OH with a VOC is
384 the rate-limiting step and ignoring non-OH sources, integrated HCHO production can be written
385 as in eqn. 7.
386 $$P_{HCHO} = \sum \alpha_i k_i [OH][X_i] = \alpha_{eff} k'_{OH} [OH] \quad (7)$$
387 Where α_i is the yield of HCHO from OH oxidation of any VOC reactant X_i and depends on both
388 the structure of X and the fate of reactive intermediates like peroxy radicals, k_i is the reaction rate
389 coefficient for VOC_i + OH, k'_{OH} represents VOC-OH reactivity, and α_{eff} is the effective yield
390 weighted over OH-VOC reactions. If all OH reactivity (including reactions with CO and NO_2)

https://doi.org/10.5194/acp-2021-389
Preprint. Discussion started: 31 May 2021


Atmospheric Chemistry and Physics Discussions

391 instead of OH-VOC reactivity is considered, α_{eff} will be about 20% smaller. As discussed by Valin
392 et al. (2016), α_{eff} from all OH reactivity is expected to range from 0.2 to 0.4 depending on the
393 magnitude of NO_x and the magnitude and speciation of VOC. The yield reported here (0.28 for all
394 OH reactivity) is on the low end of this range, implying that HCHO production in the plume is not
395 very efficient due to the nature of the emitted VOC and/or the balance of RO_2 reactions with NO,
396 HO_2, and other RO_2. High α_{eff} values reported by Valin et al. (2016) occur in high isoprene
397 emission regions, implying the emitted VOCs in wildfires are not as efficient as isoprene in
398 producing HCHO. Our α_{eff} of 0.28, when considered all OH reactivity, is higher than the value of
399 0.20 (± 0.01) derived by Wolfe et al. (2019) for total-column HCHO in the remote troposphere,
400 where methane oxidation is the primary HCHO source. The potential low bias in observed HCHO
401 could lead to a proportional (27%) low bias in in α_{eff}. We used PTRMS CH_3CHO measurements,
402 which had more complete data coverage than TOGA, and can be more easily integrated over the
403 iWAS sampling time than the TOGA CH_3CHO, which had a sampling duration between 12-33s
404 during FIREX-AQ, and was not always aligned with the iWAS time step. This could also lead to
405 slightly high bias (~5%) in the calculated OH reactivity and a low bias in the α_{eff}. This indicates
406 that besides the potential missing VOCs, the uncertainties in measured VOCs concentrations also
407 contribute to the uncertainties in OH reactivity and α_{eff}. The α_{eff} for the eastern US wildfire plume
408 seems to be higher than western US wildfire plumes but the uncertainties are large. Higher
409 NO_x/VOC ratio in the eastern than western US wildfire plumes may contribute to the higher α_{eff}
410 because more NO_x generally means more radical turnover and a larger fraction of RO_2 + NO, both
411 of which favor HCHO production.
412
413 3.4 Implications for interpretation of satellite observations

https://doi.org/10.5194/acp-2021-389
Preprint. Discussion started: 31 May 2021


Atmospheric Chemistry and Physics Discussions

The quantification of the evolution of HCHO in wildfire plumes can be leveraged to enhance interpretations of satellite remote sensing observations. The good correlation of dilution-corrected secondary HCHO production and oxidant levels suggests the use of satellite HCHO data to estimate oxidant levels in biomass burning plumes. Similar to the studies of NO_2 lifetime from satellite NO_2 data (e.g., Laughner and Cohen, 2019; Liu et al., 2016), with parameterized production rates of HCHO as a function of OH from this study, the effective lifetime of HCHO and OH concentrations in the wildfire plumes could potentially be derived from remote sensing HCHO and CO data if the photolysis rates can be properly parameterized. Satellite HCHO retrievals in biomass burning plumes remain challenging, and information about vertical distributions of trace gases and aerosols from airborne measurements are likely needed to improve satellite retrievals in biomass burning plumes. The effective yield of HCHO from this analysis indicates that the biomass burning VOCs could be less efficient than isoprene in producing HCHO, although other factors such as balance of RO_2 reactions with NO, HO_2, and other RO_2 can play a role. This information may be useful for estimating VOC emissions from satellite HCHO data.

4. Conclusions

We studied the chemical evolution of HCHO in wildfire plumes during FIREX-AQ. Twelve well-developed plumes with consistent chemical and physical age 1–6 h downwind were selected among 26 wildfire plumes sampled. During plume transport and aging, dilution-corrected HCHO increased in smoke from nine wildfires and decreased in three, depending on the balance of HCHO production and loss processes. Secondary nHCHO production tracks average OH concentrations, indicating that the variability in OH rather than the variability in the reactive VOC pool drives the

https://doi.org/10.5194/acp-2021-389
Preprint. Discussion started: 31 May 2021


Atmospheric Chemistry and Physics Discussions

437 production of nHCHO in these wildfire plumes. The effective HCHO yield from OH-initiated
438 VOC oxidation is estimated to be 0.33 (± 0.05), which is about in the middle of previous studies
439 of isoprene-rich, urban VOC-dominated and remote atmospheric background regions.

440

441

442
443

444

https://doi.org/10.5194/acp-2021-389
Preprint. Discussion started: 31 May 2021

Atmospheric Chemistry and Physics Discussions

Appendix A. Derivation of secondary nHCHO production rate from mass balance equation

Change of HCHO concentration with time can be obtained from mass balance equation (eqn. A1)

$$\frac{\mathrm{d\,HCHO}}{\mathrm{dt}} = \mathrm{P} - \mathrm{L} - \mathrm{D} \quad \text{(A1)}$$

where P is the HCHO chemical production term; L is the HCHO chemical loss term; and D is the dilution term.

Considering the HCHO normalized excess mixing ratio ($\mathrm{nHCHO} = \frac{\mathrm{HCHO}-\mathrm{HCHO_{bkg}}}{\mathrm{CO}-\mathrm{CO_{bkg}}}$) and assuming that the HCHO background change is relatively small ($\frac{\mathrm{d\,HCHO\,bkg}}{\mathrm{dt}} \approx 0$), $\frac{\mathrm{d\,HCHO}}{\mathrm{dt}}$ can be written as

$$\frac{\mathrm{d\,HCHO}}{\mathrm{dt}} = \Delta\,\mathrm{CO}\frac{\mathrm{d\,nHCHO}}{\mathrm{dt}} + \mathrm{nHCHO}\frac{\mathrm{d}\,\Delta\mathrm{CO}}{\mathrm{dt}}. \quad \text{(A2)}$$

Because L, D and P terms are as

$$\mathrm{L} = (\mathrm{J_{HCHO}} + \mathrm{k_{HCHO}}\,[\mathrm{OH}])\mathrm{HCHO}. \quad \text{(A3)}$$

$$\mathrm{D} = -\mathrm{kdil}\,(\mathrm{HCHO} - HCHO_{bkg}) = -\frac{1}{\Delta\mathrm{CO}}\frac{\mathrm{d}\,\Delta\mathrm{CO}}{\mathrm{dt}}\,\mathrm{HCHO}\,. \quad \text{(A4)}$$

$$\mathrm{P} = \frac{\mathrm{d\,HCHO}}{\mathrm{dt}} + \mathrm{L} + \mathrm{D} = \Delta\,\mathrm{CO}\frac{\mathrm{d\,nHCHO}}{\mathrm{dt}} + \mathrm{nHCHO}\frac{\mathrm{d}\,\Delta\mathrm{CO}}{\mathrm{dt}} + (\mathrm{J_{HCHO}} + \mathrm{k_{HCHO}}\,[\mathrm{OH}])\mathrm{HCHO} - \frac{1}{\Delta\mathrm{CO}}\frac{\mathrm{d}\,\Delta\mathrm{CO}}{\mathrm{dt}}\,\mathrm{HCHO}\,. \quad \text{(A5)}$$

By assuming HCHO >> HCHO bkg, $\frac{P}{\Delta CO}$ can be written as

$$\frac{P}{\Delta CO} = \frac{dnHCHO}{dt} + (\mathrm{J_{HCHO}} + \mathrm{k_{HCHO}}[OH])nHCHO. \quad \text{(A6)}$$

Where $\frac{d\,\mathrm{nHCHO}}{dt}$ can be derived from measured HCHO and CO vs physical age; $\mathrm{J_{HCHO}}$ is the HCHO photolysis coefficient, derived from in-situ actinic flux measurements; OH is calculated from VOCs ratios (Sect.2.4); $\mathrm{k_{HCHO}}$ is the reaction rate coefficient of HCHO and OH.

https://doi.org/10.5194/acp-2021-389
Preprint. Discussion started: 31 May 2021


Atmospheric Chemistry and Physics Discussions

Data and code availability:

Data are publicly available at https://www-air.larc.nasa.gov/missions/firex-aq/index.html with a dataset doi: FIREX-AQ DOI: 10.5067/SUBORBITAL/FIREXAQ2019/DATA001. F0AM is available at https://github.com/AirChem/F0AM. Model setup scripts for this study are available from the contact author upon request.

Author contribution:

GMW and TFH directed the research direction. JL analyzed the data and discussed the results with GMW. JL wrote the manuscript. TFH, GMW, JMS, JL, and RAH made ISAF HCHO measurements. JBG, AL, and VS made iWAS measurements. GSD, JBN, HSH, JPG made DACOM CO measurements. SRH and KU made CAFS photolysis frequencies measurements. CDH, CHF, and AA provided the trajectories-based plume physical age. HSH provided MCE calculation. TBR, JP, and IB made O_3 measurements. CW, MMC, GIG, and KS made PTR-ToF-MS VOC measurements. AF, DR, and PW made CAMS HCHO measurements. ECA and RSH made TOGA VOC measurements. SSB, CCW, MAR, and RAW made ACES measurements. PRV and JAN made CIMS measurements. All authors reviewed and commented on the manuscript.

Acknowledgement:

We gratefully acknowledge the crew, logistical personnel, science team and science leadership who facilitated the FIREX-AQ mission. We also thank Gao Chen and Ali Aknan for the merged DC8 dataset used in this study. JL, GMW, RAH, JMS, and TFH acknowledge support from the NASA Tropospheric Composition Program and NOAA Climate Program Office's Atmospheric Chemistry, Carbon Cycle and Climate (AC4) program (NA17OAR4310004). SRH and KU were

https://doi.org/10.5194/acp-2021-389
Preprint. Discussion started: 31 May 2021

490 funded by the NASA Tropospheric Composition Program (80NSSC18K0638). This material is
491 based upon work supported by the National Center for Atmospheric Research, which is a major
492 facility sponsored by the National Science Foundation under Cooperative Agreement No. 1852977.
493 KS acknowledges the support from the fund a Grant-in-Aid for Scientific Research (C) (18K05179)
494 from the Ministry of Education, Culture, Sports, Science and Technology of Japan.

495

496

497

498 Figures:

https://doi.org/10.5194/acp-2021-389
Preprint. Discussion started: 31 May 2021

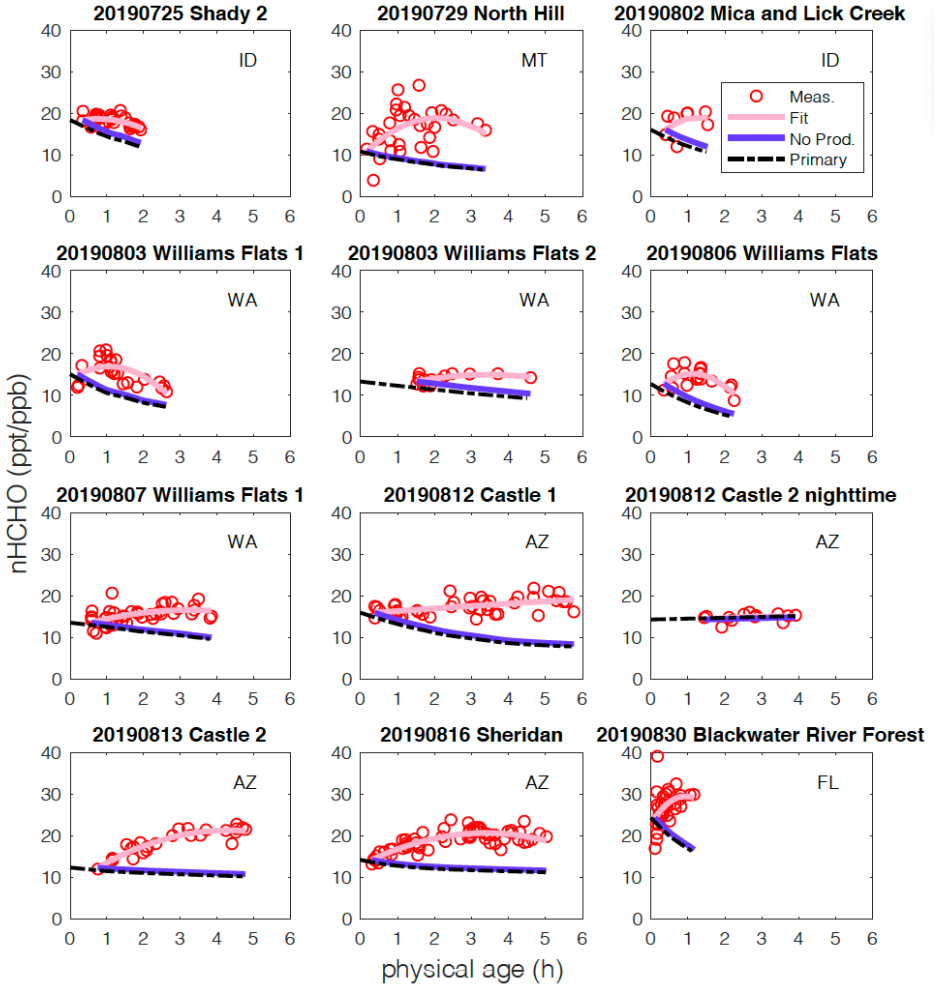

Figure 1. Observed nHCHO (HCHO to CO NEMR) trends (red circle), quadratic polynomial fit (pink curve), calculated decay of nHCHO trend without secondary production (blue curve) using measured photolysis rates, and calculated primary nHCHO trends (black dashed curve) with physical age for the 12 wildfire plumes. The state of fire location for each fire plume is listed.

https://doi.org/10.5194/acp-2021-389
Preprint. Discussion started: 31 May 2021

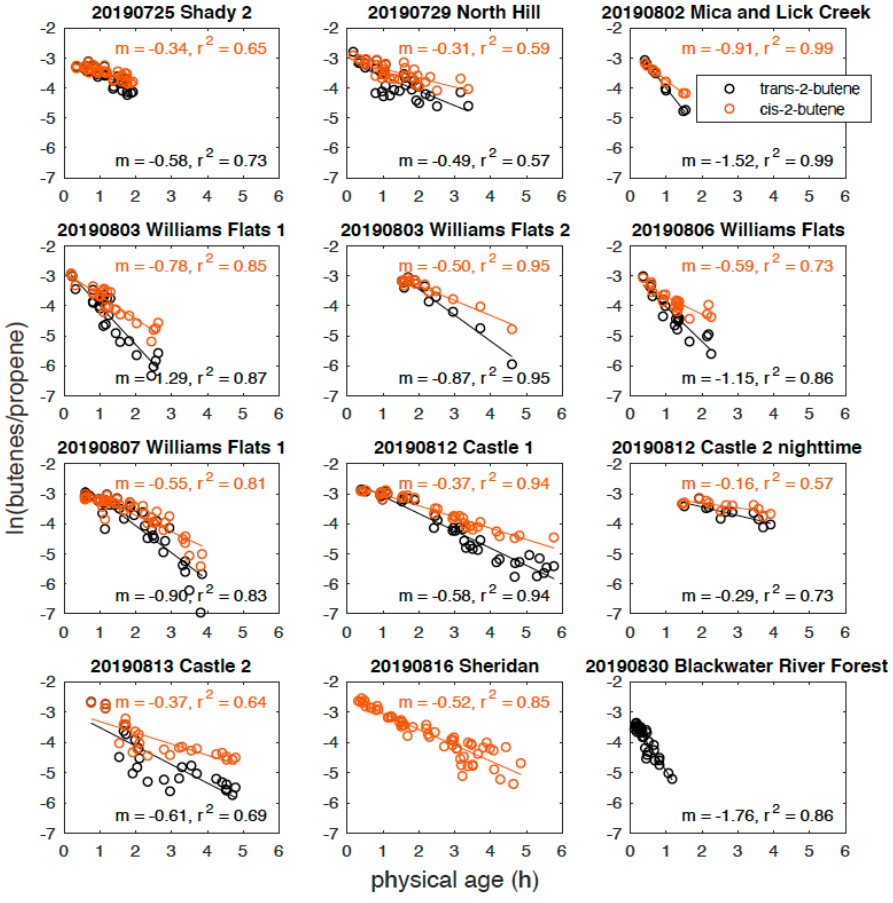

Figure 2. Natural logarithms of cis-2-butene to propene ratios (red circles) and trans-2-butene to propene ratios (black circles) vs. physical age for 12 wildfire plumes. The natural logarithms of the butenes/propene ratios correlate well with physical age with correlation coefficients, r^2, ≥ 0.57. The slopes of the linear fits to the data (m, shown on the plots) reflect the oxidation by OH and O_3 and are used to calculate the average OH concentrations with average O_3 concentrations and reaction rate coefficients.

https://doi.org/10.5194/acp-2021-389
Preprint. Discussion started: 31 May 2021

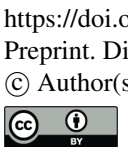

Atmospheric Chemistry and Physics Discussions

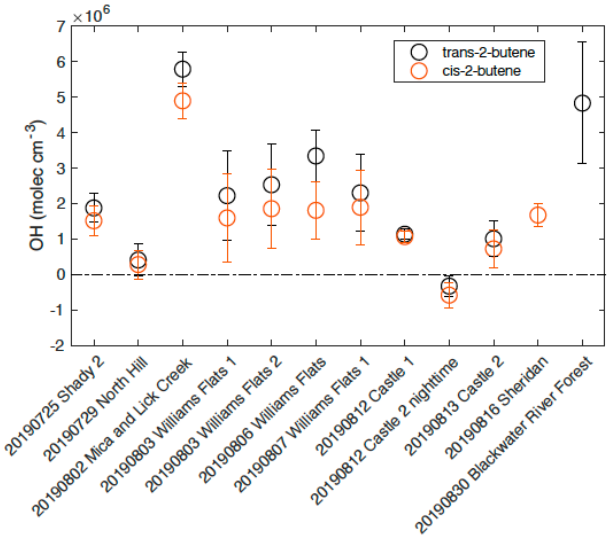

514

515 Figure 3. Estimated average OH concentrations for the plumes analyzed from the decay of trans-
516 2-butene – propene (black) and the decay of cis-2-butene – propene (red). The error bars represent
517 the propagated uncertainties from the slopes of butenes – propene decay and ozone variability
518 within the plume.

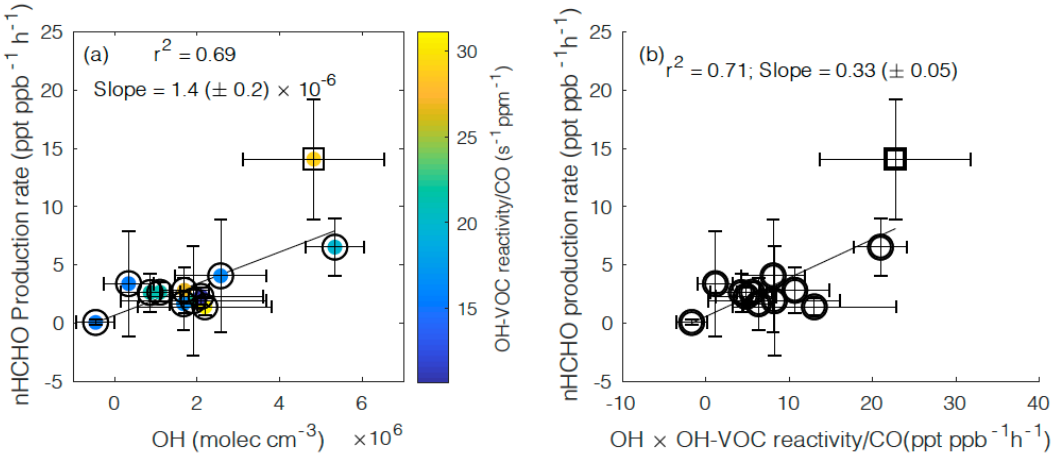

519
520

521 Figure 4. (a) Average secondary nHCHO production rate vs. average OH concentration, color-
522 coded by OH-VOC reactivity, for the 12 plumes including 11 western US wildfire plumes (circles)

https://doi.org/10.5194/acp-2021-389
Preprint. Discussion started: 31 May 2021


Atmospheric Chemistry and Physics Discussions

and 1 eastern US wildfire plume (square). An uncertainty weighted linear York regression (Derek, 1968) yields a slope = 1.4 ($\pm$0.2)$\times$ 10^{-6} and r^2 = 0.69 for the 12 wildfire plumes. (b) Average secondary nHCHO production rate vs. the average product of OH and OH-VOC reactivity normalized to CO (OH$\times$ OH-VOC reactivity/CO) for each plume. An uncertainty weighted linear York regression yields a slope = 0.33 ($\pm$ 0.05) and r^2 = 0.71. The slope represents the estimated effective yield α_{eff} of HCHO per VOC molecule oxidized by OH for the US wildfires.

https://doi.org/10.5194/acp-2021-389
Preprint. Discussion started: 31 May 2021


Atmospheric Chemistry and Physics Discussions

531 Reference

532 Akagi, S. K., Yokelson, R. J., Wiedinmyer, C., Alvarado, M., Reid, J. S., Karl, T., Crounse, J. D.
533 and Wennberg, P. O.: ScholarWorks at University of Montana Emission Factors for Open and
534 Domestic Biomass Burning for Use in Atmospheric Models Let us know how access to this
535 document benefits you ., 2011.
536 Alvarado, L. M. A., Richter, A., Vrekoussis, M., Hilboll, A., Kalisz Hedegaard, A. B.,
537 Schneising, O. and Burrows, J. P.: Unexpected long-range transport of glyoxal and formaldehyde
538 observed from the Copernicus Sentinel-5 Precursor satellite during the 2018 Canadian wildfires,
539 Atmos. Chem. Phys., 20(4), 2057–2072, doi:10.5194/acp-20-2057-2020, 2020.
540 Alvarado, M. J., Logan, J. A., Mao, J., Apel, E., Riemer, D., Blake, D., Cohen, R. C., Min, K. E.,
541 Perring, A. E., Browne, E. C., Wooldridge, P. J., Diskin, G. S., Sachse, G. W., Fuelberg, H.,
542 Sessions, W. R., Harrigan, D. L., Huey, G., Liao, J., Case-Hanks, A., Jimenez, J. L., Cubison, M.
543 J., Vay, S. A., Weinheimer, A. J., Knapp, D. J., Montzka, D. D., Flocke, F. M., Pollack, I. B.,
544 Wennberg, P. O., Kurten, A., Crounse, J., St. Clair, J. M., Wisthaler, A., Mikoviny, T., Yantosca,
545 R. M., Carouge, C. C. and Le Sager, P.: Nitrogen oxides and PAN in plumes from boreal fires
546 during ARCTAS-B and their impact on ozone: An integrated analysis of aircraft and satellite
547 observations, Atmos. Chem. Phys., 10(20), 9739–9760, doi:10.5194/acp-10-9739-2010, 2010.
548 Apel, E. C., Hornbrook, R. S., Hills, A. J., Blake, N. J., Barth, M. C., Weinheimer, A., Cantrell,
549 C., Rutledge, S. A., Basarab, B., Crawford, J., Diskin, G., Homeyer, C. R., Campos, T., Flocke,
550 F., Fried, A., Blake, D. R., Brune, W., Pollack, I., Peischl, J., Ryerson, T., Wennberg, P. O.,
551 Crounse, J. D., Wisthaler, A., Mikoviny, T., Huey, G., Heikes, B., Sullivan, D. O. and Riemer,
552 D. D.: Journal of Geophysical Research : Atmospheres, , (x), 2505–2523,
553 doi:10.1002/2014JD022121.Received, 2015.

https://doi.org/10.5194/acp-2021-389
Preprint. Discussion started: 31 May 2021


Atmospheric Chemistry and Physics Discussions

554 Atkinson, R., Baulch, D. L., Cox, R. A., Crowley, J. N., Hampson, R. F., Hynes, R. G., Jenkin,
555 M. E., Rossi, M. J., Troe, J. and IUPAC Subcommittee: Evaluated kinetic and photochemical
556 data for atmospheric chemistry: Volume II – gas phase reactions of organic species, Atmos.
557 Chem. Phys, 6, 3625–4055, doi:https://doi.org/10.5194/acp-6-3625-2006, 2006.
558 Bourgeois, I., Peischl, J., Thompson, C. R., Aikin, K. C., Campos, T., Clark, H., Commane, R.,
559 Daube, B., Diskin, G. W., Elkins, J. W., Gao, R. S., Gaudel, A., Hintsa, E. J., Johnson, B. J.,
560 Kivi, R., McKain, K., Moore, F. L., Parrish, D. D., Querel, R., Ray, E., Sánchez, R., Sweeney,
561 C., Tarasick, D. W., Thompson, A. M., Thouret, V., Witte, J. C., Wofsy, S. C. and Ryerson, T.
562 B.: Global-scale distribution of ozone in the remote troposphere from the ATom and HIPPO
563 airborne field missions, Atmos. Chem. Phys., 20(17), 10611–10635, doi:10.5194/acp-20-10611-
564 2020, 2020.
565 Cazorla, M., Wolfe, G. M., Bailey, S. A., Swanson, A. K., Arkinson, H. L. and Hanisco, T. F.: A
566 new airborne laser-induced fluorescence instrument for in situ detection of formaldehyde
567 throughout the troposphere and lower stratosphere, Atmos. Meas. Tech., 8(2), 541–552,
568 doi:10.5194/amt-8-541-2015, 2015.
569 Coggon, M. M., Lim, C. Y., Koss, A. R., Sekimoto, K., Yuan, B., Gilman, J. B., Hagan, D. H.,
570 Selimovic, V., Zarzana, K. J., Brown, S. S., M Roberts, J., Müller, M., Yokelson, R., Wisthaler,
571 A., Krechmer, J. E., Jimenez, J. L., Cappa, C., Kroll, J. H., De Gouw, J. and Warneke, C.: OH
572 chemistry of non-methane organic gases (NMOGs) emitted from laboratory and ambient
573 biomass burning smoke: Evaluating the influence of furans and oxygenated aromatics on ozone
574 and secondary NMOG formation, Atmos. Chem. Phys., 19(23), 14875–14899, doi:10.5194/acp-
575 19-14875-2019, 2019.
576 Decker, Z. C. J., Zarzana, K. J., Coggon, M., Min, K. E., Pollack, I., Ryerson, T. B., Peischl, J.,

https://doi.org/10.5194/acp-2021-389
Preprint. Discussion started: 31 May 2021


Atmospheric Chemistry and Physics Discussions

577 Edwards, P., Dubé, W. P., Markovic, M. Z., Roberts, J. M., Veres, P. R., Graus, M., Warneke,
578 C., De Gouw, J., Hatch, L. E., Barsanti, K. C. and Brown, S. S.: Nighttime Chemical
579 Transformation in Biomass Burning Plumes: A Box Model Analysis Initialized with Aircraft
580 Observations, Environ. Sci. Technol., 53(5), 2529–2538, doi:10.1021/acs.est.8b05359, 2019.
581 Derek, Y.: Least-squares fitting of a straight line, Can. J. Phys., 46(16), 1845–1847,
582 doi:10.1139/p68-523, 1968.
583 Fu, T. M., Jacob, D. J., Palmer, P. I., Chance, K., Wang, Y. X., Barletta, B., Blake, D. R.,
584 Stanton, J. C. and Pilling, M. J.: Space-based formaldehyde measurements as constrains on
585 volatile organic compound emissions in east and south Asia and implications for ozone, J.
586 Geophys. Res. Atmos., 112(6), 1–15, doi:10.1029/2006JD007853, 2007.
587 Garofalo, L. A., Pothier, M. A., Levin, E. J. T., Campos, T., Kreidenweis, S. M. and Farmer, D.
588 K.: Emission and Evolution of Submicron Organic Aerosol in Smoke from Wildfires in the
589 Western United States, ACS Earth Sp. Chem., 3(7), 1237–1247,
590 doi:10.1021/acsearthspacechem.9b00125, 2019.
591 Gilman, J. B., Lerner, B. M., Kuster, W. C., Goldan, P. D., Warneke, C., Veres, P. R., Roberts, J.
592 M., De Gouw, J. A., Burling, I. R. and Yokelson, R. J.: Biomass burning emissions and potential
593 air quality impacts of volatile organic compounds and other trace gases from fuels common in
594 the US, Atmos. Chem. Phys., 15(24), 13915–13938, doi:10.5194/acp-15-13915-2015, 2015.
595 Hall, S. R., Ullmann, K., Prather, M. J., Flynn, C. M., Murray, L. T., Fiore, A. M., Correa, G.,
596 Strode, S. A., Steenrod, S. D., Lamarque, J. F., Guth, J., Josse, B., Flemming, J., Huijnen, V.,
597 Luke Abraham, N. and Archibald, A. T.: Cloud impacts on photochemistry: Building a
598 climatology of photolysis rates from the Atmospheric Tomography mission, Atmos. Chem.
599 Phys., 18(22), 16809–16828, doi:10.5194/acp-18-16809-2018, 2018.

https://doi.org/10.5194/acp-2021-389
Preprint. Discussion started: 31 May 2021


Atmospheric Chemistry and Physics Discussions

600 Jaffe, D. A. and Wigder, N. L.: Ozone production from wildfires: A critical review, Atmos.
601 Environ., 51, 1–10, doi:10.1016/j.atmosenv.2011.11.063, 2012.
602 Jenkin, M. E., Young, J. C. and Rickard, A. R.: The MCM v3.3.1 degradation scheme for
603 isoprene, Atmos. Chem. Phys., 15(20), 11433–11459, doi:10.5194/acp-15-11433-2015, 2015.
604 Kaiser, J., Jacob, D. J., Zhu, L., Travis, K. R., Fisher, J. A., González Abad, G., Zhang, L.,
605 Zhang, X., Fried, A., Crounse, J. D., Clair, J. M. S. and Wisthaler, A.: High-resolution inversion
606 of OMI formaldehyde columns to quantify isoprene emission on ecosystem-relevant scales:
607 Application to the southeast US, Atmos. Chem. Phys., 18(8), 5483–5497, doi:10.5194/acp-18-
608 5483-2018, 2018.
609 Koss, A. R., Sekimoto, K., Gilman, J. B., Selimovic, V., Coggon, M. M., Zarzana, K. J., Yuan,
610 B., Lerner, B. M., Brown, S. S., Jimenez, J. L., Krechmer, J., Roberts, J. M., Warneke, C.,
611 Yokelson, R. J. and De Gouw, J.: Non-methane organic gas emissions from biomass burning:
612 Identification, quantification, and emission factors from PTR-ToF during the FIREX 2016
613 laboratory experiment, Atmos. Chem. Phys., 18(5), 3299–3319, doi:10.5194/acp-18-3299-2018,
614 2018.
615 Laughner, J. and Cohen, R. C.: Direct observation of changing NO, Science (80-.)., 727(x),
616 723–727, 2019.
617 Lerner, B. M., Gilman, J. B., Aikin, K. C., Atlas, E. L., Goldan, P. D., Graus, M., Hendershot,
618 R., Isaacman-Vanwertz, G. A., Koss, A., Kuster, W. C., Lueb, R. A., Mclaughlin, R. J., Peischl,
619 J., Sueper, D., Ryerson, T. B., Tokarek, T. W., Warneke, C., Yuan, B. and De Gouw, J. A.: An
620 improved, automated whole air sampler and gas chromatography mass spectrometry analysis
621 system for volatile organic compounds in the atmosphere, Atmos. Meas. Tech., 10(1), 291–313,
622 doi:10.5194/amt-10-291-2017, 2017.

https://doi.org/10.5194/acp-2021-389
Preprint. Discussion started: 31 May 2021


Atmospheric Chemistry and Physics Discussions

623 Liao, J., Hanisco, T. F., Wolfe, G. M., St. Clair, J., Jimenez, J. L., Campuzano-Jost, P., Nault, B.
624 A., Fried, A., Marais, E. A., Gonzalez Abad, G., Chance, K., Jethva, H. T., Ryerson, T. B.,
625 Warneke, C. and Wisthaler, A.: Towards a satellite – in situ hybrid estimate for
626 organic aerosol abundance, Atmos. Chem. Phys. Discuss., 1–51, doi:10.5194/acp-2018-651,
627 2019.
628 Liu, F., Beirle, S., Zhang, Q., Dörner, S., He, K. and Wagner, T.: NOx lifetimes and emissions of
629 cities and power plants in polluted background estimated by satellite observations, Atmos.
630 Chem. Phys., 16(8), 5283–5298, doi:10.5194/acp-16-5283-2016, 2016.
631 Liu, X., Huey, L. G., Yokelson, R. J., Selimovic, V., Simpson, I. J., Müller, M., Jimenez, J. L.,
632 Campuzano-Jost, P., Beyersdorf, A. J., Blake, D. R., Butterfield, Z., Choi, Y., Crounse, J. D.,
633 Day, D. A., Diskin, G. S., Dubey, M. K., Fortner, E., Hanisco, T. F., Hu, W., King, L. E.,
634 Kleinman, L., Meinardi, S., Mikoviny, T., Onasch, T. B., Palm, B. B., Peischl, J., Pollack, I. B.,
635 Ryerson, T. B., Sachse, G. W., Sedlacek, A. J., Shilling, J. E., Springston, S., St. Clair, J. M.,
636 Tanner, D. J., Teng, A. P., Wennberg, P. O., Wisthaler, A. and Wolfe, G. M.: Airborne
637 measurements of western U.S. wildfire emissions: Comparison with prescribed burning and air
638 quality implications, J. Geophys. Res., 122(11), 6108–6129, doi:10.1002/2016JD026315, 2017.
639 Majdi, M., Sartelet, K., Maria Lanzafame, G., Couvidat, F., Kim, Y., Chrit, M. and Turquety, S.:
640 Precursors and formation of secondary organic aerosols from wildfires in the Euro-
641 Mediterranean region, Atmos. Chem. Phys., 19(8), 5543–5569, doi:10.5194/acp-19-5543-2019,
642 2019.
643 Marais, E. A., Jacob, D. J., Guenther, A., Chance, K., Kurosu, T. P., Murphy, J. G., Reeves, C.
644 E. and Pye, H. O. T.: Improved model of isoprene emissions in Africa using Ozone Monitoring
645 Instrument (OMI) satellite observations of formaldehyde: Implications for oxidants and

https://doi.org/10.5194/acp-2021-389
Preprint. Discussion started: 31 May 2021


Atmospheric Chemistry and Physics Discussions

646 particulate matter, Atmos. Chem. Phys., 14(15), 7693–7703, doi:10.5194/acp-14-7693-2014,
647 2014.
648 Mauzerall, D. L., Logan, J. A., Jacob, D. J., Anderson, B. E., Blake, D. R., Bradshaw, J. D.,
649 Heikes, B., Sachse, G. W., Singh, H. and Talbot, B.: Photochemistry in biomass burning plumes
650 and implications for tropospheric ozone over the tropical South Atlantic, J. Geophys. Res.
651 Atmos., 103(D7), 8401–8423, doi:10.1029/97JD02612, 1998.
652 Meller, R. and Moortgat, G. K.: Temperature dependence of the absorption cross sections of
653 formaldehyde between 223 and 323 K in the wavelength range 225-375 nm, J. Geophys. Res.
654 Atmos., 105(D6), 7089–7101, doi:10.1029/1999JD901074, 2000.
655 Millet, D. B., Jacob, D. J., Boersma, K. F., Fu, T. M., Kurosu, T. P., Chance, K., Heald, C. L.
656 and Guenther, A.: Spatial distribution of isoprene emissions from North America derived from
657 formaldehyde column measurements by the OMI satellite sensor, J. Geophys. Res. Atmos.,
658 113(2), 1–18, doi:10.1029/2007JD008950, 2008.
659 Min, K. E., Washenfelder, R. A., Dubé, W. P., Langford, A. O., Edwards, P. M., Zarzana, K. J.,
660 Stutz, J., Lu, K., Rohrer, F., Zhang, Y. and Brown, S. S.: A broadband cavity enhanced
661 absorption spectrometer for aircraft measurements of glyoxal, methylglyoxal, nitrous acid,
662 nitrogen dioxide, and water vapor, Atmos. Meas. Tech., 9(2), 423–440, doi:10.5194/amt-9-423-
663 2016, 2016.
664 Müller, M., Anderson, B. E., Beyersdorf, A. J., Crawford, J. H., Diskin, G. S., Eichler, P., Fried,
665 A., Keutsch, F. N., Mikoviny, T., Thornhill, K. L., Walega, J. G., Weinheimer, A. J., Yang, M.,
666 Yokelson, R. J. and Wisthaler, A.: In situ measurements and modeling of reactive trace gases in
667 a small biomass burning plume, Atmos. Chem. Phys., 16(6), 3813–3824, doi:10.5194/acp-16-
668 3813-2016, 2016.

https://doi.org/10.5194/acp-2021-389
Preprint. Discussion started: 31 May 2021


Atmospheric Chemistry and Physics Discussions

669 Palm, B. B., Peng, Q., Fredrickson, C. D., Lee, B. H., Garofalo, L. A. and Pothier, M. A.:
670 Quantification of organic aerosol and brown carbon evolution in fresh wildfire plumes, ,
671 doi:10.1073/pnas.2012218117, 2020.
672 Peng, Q., Palm, B. B., Melander, K. E., Lee, B. H., Hall, S. R., Ullmann, K., Campos, T.,
673 Weinheimer, A. J., Apel, E. C., Hornbrook, R. S., Hills, A. J., Montzka, D. D., Flocke, F., Hu,
674 L., Permar, W., Wielgasz, C., Lindaas, J., Pollack, I. B., Fischer, E. V., Bertram, T. H. and
675 Thornton, J. A.: HONO Emissions from Western U.S. Wildfires Provide Dominant Radical
676 Source in Fresh Wildfire Smoke, Environ. Sci. Technol., 54(10), 5954–5963,
677 doi:10.1021/acs.est.0c00126, 2020.
678 R. J. Yokelson, J. G. Goode, l D. E. Ward, R. A. Susott, R. E. Babbitt, D. D. Wade, I. Bertschi,
679 D. W. T. Griffith, and W. M. H.: Emissions of formaldehyde, acetic acid, methanol, and other
680 trace gases from biomass fires in North Carolina measured by airborne Fourier transform
681 infrared spectroscopy, J. Geophys. Res. Atmos., 104(D23), 30109–30125,
682 doi:10.1029/1999JD900817, 1999.
683 Richter, D., Weibring, P., Walega, J. G., Fried, A., Spuler, S. M. and Taubman, M. S.: CAMS -
684 Compact atmospheric multi-species spectrometer, Conf. Lasers Electro-Optics Eur. - Tech. Dig.,
685 2015-Augus, 5–6, 2015.
686 Sachse, G. W., Collins, Jr., J. E., Hill, G. F., Wade, L. O., Burney, L. G. and Ritter, J. A.:
687 Airborne tunable diode laser sensor for high-precision concentration and flux measurements of
688 carbon monoxide and methane, Meas. Atmos. Gases, 1433(May 1991), 157,
689 doi:10.1117/12.46162, 1991.
690 Sander, S. P., Abbatt, J., Barker, J. R., Burkholder, J. B., Friedl, R. R., Golden, D. M., Huie, R.
691 E., Kolb, C. E., Kurylo, M. J., Moortgat, G. K., Orkin, V. L. and Wine, P. H.: Chemical Kinetics

https://doi.org/10.5194/acp-2021-389
Preprint. Discussion started: 31 May 2021


Atmospheric Chemistry and Physics Discussions

692 and Photochemical Data for Use in Atmospheric Studies Evaluation Number 17, JPL Publ. 10-6,
693 Jet Propul [online] Available from: http://jpldataeval.jpl.nasa.gov/, 2011.
694 Simpson, I. J., Akagi, S. K., Barletta, B., Blake, N. J., Choi, Y., Diskin, G. S., Fried, A.,
695 Fuelberg, H. E., Meinardi, S., Rowland, F. S., Vay, S. A., Weinheimer, A. J., Wennberg, P. O.,
696 Wiebring, P., Wisthaler, A., Yang, M., Yokelson, R. J. and Blake, D. R.: Boreal forest fire
697 emissions in fresh Canadian smoke plumes: C1-C10 volatile organic compounds (VOCs), CO2,
698 CO, NO2, NO, HCN and CH3CN, Atmos. Chem. Phys., 11(13), 6445–6463, doi:10.5194/acp-
699 11-6445-2011, 2011.
700 De Smedt, I., Theys, N., Yu, H., Danckaert, T., Lerot, C., Compernolle, S., Van Roozendael, M.,
701 Richter, A., Hilboll, A., Peters, E., Pedergnana, M., Loyola, D., Beirle, S., Wagner, T., Eskes, H.,
702 Van Geffen, J., Folkert Boersma, K. and Veefkind, P.: Algorithm theoretical baseline for
703 formaldehyde retrievals from S5P TROPOMI and from the QA4ECV project, Atmos. Meas.
704 Tech., 11(4), 2395–2426, doi:10.5194/amt-11-2395-2018, 2018.
705 Stavrakou, T., Müller, J. F., De Smedt, I., Van Roozendael, M., Van Der Werf, G. R., Giglio, L.
706 and Guenther, A.: Global emissions of non-methane hydrocarbons deduced from SCIAMACHY
707 formaldehyde columns through 2003-2006, Atmos. Chem. Phys., 9(11), 3663–3679,
708 doi:10.5194/acp-9-3663-2009, 2009.
709 Trentmann, J., Yokelson, R. J., Hobbs, P. V., Winterrath, T., Christian, T. J., Andreae, M. O. and
710 Mason, S. A.: An analysis of the chemical processes in the smoke plume from a savanna fire, J.
711 Geophys. Res. D Atmos., 110(12), 1–20, doi:10.1029/2004JD005628, 2005.
712 Valin, L. C., Fiore, A. M., Chance, K. and Abad, G. G.: Journal of geophysical research, J.
713 Geophys. Res. Atmos., 175(4449), 238, doi:10.1038/175238c0, 2016.
714 Veres, P. R., Andrew Neuman, J., Bertram, T. H., Assaf, E., Wolfe, G. M., Williamson, C. J.,

https://doi.org/10.5194/acp-2021-389
Preprint. Discussion started: 31 May 2021


Atmospheric Chemistry and Physics Discussions

715 Weinzierl, B., Tilmes, S., Thompson, C. R., Thames, A. B., Schroder, J. C., Saiz-Lopez, A.,
716 Rollins, A. W., Roberts, J. M., Price, D., Peischl, J., Nault, B. A., Møller, K. H., Miller, D. O.,
717 Meinardi, S., Li, Q., Lamarque, J. F., Kupc, A., Kjaergaard, H. G., Kinnison, D., Jimenez, J. L.,
718 Jernigan, C. M., Hornbrook, R. S., Hills, A., Dollner, M., Day, D. A., Cuevas, C. A.,
719 Campuzano-Jost, P., Burkholder, J., Paul Bui, T., Brune, W. H., Brown, S. S., Brock, C. A.,
720 Bourgeois, I., Blake, D. R., Apel, E. C. and Ryerson, T. B.: Global airborne sampling reveals a
721 previously unobserved dimethyl sulfide oxidation mechanism in the marine atmosphere, Proc.
722 Natl. Acad. Sci. U. S. A., 117(9), 4505–4510, doi:10.1073/pnas.1919344117, 2020.
723 Warneke, C., McKeen, S. A., de Gouw, J. A., Goldan, P. D., Kuster, W. C., Holloway, J. S.,
724 Williams, E. J., Lerner, B. M., Parrish, D. D., Trainer, M., Fehsenfeld, F. C., Kato, S., Atlas, E.
725 L., Baker, A. and Blake, D. R.: Determination of urban volatile organic compound emission
726 ratios and comparison with an emissions database, J. Geophys. Res. Atmos., 112(10),
727 doi:10.1029/2006JD007930, 2007.
728 Westerling, A. L., Hidalgo, H. G., Cayan, D. R. and Swetnam, T. W.: Warming and earlier
729 spring increase Western U.S. forest wildfire activity, Science (80-.)., 313(5789), 940–943,
730 doi:10.1126/science.1128834, 2006.
731 Wiggins, E. B., Soja, A. J., Gargulinski, E., Halliday, H. S., Pierce, R. B., Schmidt, C. C.,
732 Nowak, J. B., DiGangi, J. P., Diskin, G. S., Katich, J. M., Perring, A. E., Schwarz, J. P.,
733 Anderson, B. E., Chen, G., Crosbie, E. C., Jordan, C., Robinson, C. E., Sanchez, K. J., Shingler,
734 T. J., Shook, M., Thornhill, K. L., Winstead, E. L., Ziemba, L. D. and Moore, R. H.: High
735 Temporal Resolution Satellite Observations of Fire Radiative Power Reveal Link Between Fire
736 Behavior and Aerosol and Gas Emissions, Geophys. Res. Lett., 47(23),
737 doi:10.1029/2020GL090707, 2020.

https://doi.org/10.5194/acp-2021-389
Preprint. Discussion started: 31 May 2021


Atmospheric Chemistry and Physics Discussions

738 Wolfe, G. M., Marvin, M. R., Roberts, S. J., Travis, K. R. and Liao, J.: The framework for 0-D
739 atmospheric modeling (F0AM) v3.1, Geosci. Model Dev., 9(9), 3309–3319, doi:10.5194/gmd-9-
740 3309-2016, 2016.
741 Wolfe, G. M., Nicely, J. M., Clair, J. M. S., Hanisco, T. F., Liao, J., Oman, L. D., Brune, W. B.,
742 Miller, D., Thames, A., Abad, G. G., Ryerson, T. B., Thompson, C. R., Peischl, J., McKain, K.,
743 Sweeney, C., Wennberg, P. O., Kim, M., Crounse, J. D., Hall, S. R., Ullmann, K., Diskin, G.,
744 Bui, P., Chang, C. and Dean-Day, J.: Correction: Mapping hydroxyl variability throughout the
745 global remote troposphere via synthesis of airborne and satellite formaldehyde observations
746 (Proceedings of the National Academy of Sciences of the United States of America (2019) 116
747 (11171–11180) D, Proc. Natl. Acad. Sci. U. S. A., 116(26), 13144,
748 doi:10.1073/pnas.1908931116, 2019.
749 Wotawa, G. and Trainer, M.: The influence of Canadian forest fires on pollutant concentrations
750 in the United States, Science (80-.)., 288(5464), 324–328, doi:10.1126/science.288.5464.324,
751 2000.
752 Yuan, B., Koss, A., Warneke, C., Gilman, J. B., Lerner, B. M., Stark, H. and De Gouw, J. A.: A
753 high-resolution time-of-flight chemical ionization mass spectrometer utilizing hydronium ions
754 (H3O+ ToF-CIMS) for measurements of volatile organic compounds in the atmosphere, Atmos.
755 Meas. Tech., 9(6), 2735–2752, doi:10.5194/amt-9-2735-2016, 2016.
756